

Article

# Lamination Texture and Its Effects on Reservoir and Geochemical Properties of the Palaeogene Kongdian Formation in the Cangdong Sag, Bohai Bay Basin, China

Mengying Li <sup>1</sup> , Songtao Wu <sup>1,2,\*</sup>, Suyun Hu <sup>1,2</sup>, Rukai Zhu <sup>1</sup>, Siwei Meng <sup>1</sup> and Jingru Yang <sup>1</sup>

- <sup>1</sup> Research Institute of Petroleum Exploration and Development (RIPED), China National Petroleum Corporation (CNPC), Beijing 100083, China; limy0301@163.com (M.L.); husy@petrochina.com.cn (S.H.); zrk@petrochina.com.cn (R.Z.); mengsw@petrochina.com.cn (S.M.); yangjingruyjr@163.com (J.Y.)  
<sup>2</sup> National Energy Tight Oil and Gas R&D Center, Beijing 100083, China  
\* Correspondence: wust@petrochina.com.cn

**Abstract:** The characteristics of laminae are critical to lacustrine shale strata. They are the keys to the quality of source rocks and reservoirs, as well as engineering operations in shale plays. This study uses organic geochemistry, thin section identification, X-ray diffraction, field emission scanning electron microscopy, and other analytical methods, to reveal the detailed lamination texture and vertical distribution of laminae in the second Member of the Kongdian Formation in Cangdong Sag. The principal results are as follows: (1) A classification of laminae is proposed to characterize reservoir and geochemical properties. The five types of laminae are as follows: feldspar-quartz laminae (FQL), clay laminae (CLL), carbonate laminae (CAL), organic matter laminae (OML), and bioclastic laminae (BCL). There are also four significant lamina combinations (with the increasing TOC values): FQL-CLL combination, FQL-CLL-BCL combination, FQL-CLL-OML combination, and FQL-CAL-CLL-OML combination; (2) differences between laminae occur because of the variability in pore types and structures. There appears to be a greater abundance of intercrystalline pores of clay minerals in the FQL, CAL, BCL, and OML, and well-developed organic pores in the CAL and CLL, and the counterparts of intragranular pores of bioclastic material in the BCL. This detailed characterization provides the following comparative quantification of the thin section porosity of laminae in the second Member of the Kongdian Formation can be differentiated: CAL > FQL > OML > BCL > CLL; (3) differentiation between vertical distributions of laminae is carried out in a single well. The FQL and CLL are widely distributed in all the samples, while the BCL is concentrated in the upper part of the second Member of the Kongdian Formation, and CAL is concentrated in the lower part. This detailed classification method, using geochemical analysis and vertical distribution descriptions, offers a detailed understanding of lamination texture and its effects on reservoir and geochemical properties, which will provide a scientific guidance and technical support to better estimate reservoir quality and to identify new sweet spots in the second Member of the Kongdian Formation in the Cangdong Sag.

**Keywords:** unconventional geology; lacustrine shale oil; sweet spot; fine-grained sedimentary; nano-pores



**Citation:** Li, M.; Wu, S.; Hu, S.; Zhu, R.; Meng, S.; Yang, J. Lamination Texture and Its Effects on Reservoir and Geochemical Properties of the Palaeogene Kongdian Formation in the Cangdong Sag, Bohai Bay Basin, China. *Minerals* **2021**, *11*, 1360. <https://doi.org/10.3390/min11121360>

Academic Editor: Thomas Gentzis

Received: 19 October 2021  
Accepted: 29 November 2021  
Published: 1 December 2021

**Publisher's Note:** MDPI stays neutral with regard to jurisdictional claims in published maps and institutional affiliations.



**Copyright:** © 2021 by the authors. Licensee MDPI, Basel, Switzerland. This article is an open access article distributed under the terms and conditions of the Creative Commons Attribution (CC BY) license (<https://creativecommons.org/licenses/by/4.0/>).

## 1. Introduction

Lacustrine shale oil is a generic term for liquid hydrocarbons and various types of organic matter that occur in lacustrine organic matter shale strata with burial depths greater than 300 m and Ro values greater than 0.5% [1–4]. Lacustrine shale oil occurs widely developed in the Ordos Basin, Junggar Basin, Songliao Basin, and Bohai Bay Basin in China. China Petrochemical Corporation estimated a total of  $145 \times 10^8$  tons of oil technically recoverable in shale play [4–6], making shale oil an important successor for oil and gas development in the future [7,8].

As a key characteristic sedimentary texture, the laminae are the most basic unit of the sedimentary layers in lacustrine shale strata. They can be observed with the naked eye [9]. In recent years, some studies have been carried out on shale laminae [10–12], focusing mainly on their scale, type, and genesis. Laminae are generally divided into a number of categories based on scale. The primary definition of laminae is original sedimentary layers which are smaller than 10 mm, and they are subdivided into thick laminae (3–10 mm) and thin laminae ( $\leq 3$  mm) [13]. Others have different methods. One of the classifications is ‘sheet’ (<1 mm), ‘laminae’ (1 mm–1 cm), ‘thin laminae’ (1 cm–10 cm), and ‘bed’ (10 cm–50 cm) [14]. Additionally, Liu et al. [15] placed the demarcation point between ‘laminae’ and ‘bed’ at 1 mm (laminae < 1 mm, bed  $\geq 1$  mm). Mineral composition is generally the most popular method for classifying laminae for unconventional studies. The Chang 7<sub>3</sub> sub-member in the Ordos Basin was identified as having four major types of laminae: tuff-rich laminae, organic-rich laminae, silt-sized feldspar-quartz laminae, and clay laminae [16]. Another method divided shales in the Yanchang Formation into ‘dark’ laminae (mostly clay minerals) and ‘bright’ laminae (clastic minerals such as quartz and feldspar) [9], and distinguished organic matter laminae, organic-rich laminae, and clay laminae in the Longmaxi Formation in the Sichuan Basin from the sedimentary conditions and mineral content variations of different laminae [17]. Furthermore, other studies have focused on the morphology and grain size differences between laminae. Campbell et al. [10] divided the laminae into ‘planar’, ‘wavy’, and ‘curved’ types according to the continuity, shape, and geometry of the black fine-grained sedimentary units. Yawar et al. [18] demarcated the black shale into mud beds and silt beds according to the differences in grain size. In terms of genetic mechanisms, some studies suggested that the formation of mud laminae and silt laminae may be related to the flourishing of silicon-rich organisms. Mud laminae is formed during the intermittent periods, and silt laminae is formed during the blooming periods [19]. A different view from the perspective of basin evolution suggested that climate change and terrigenous clastic supply intensity have influenced the vertical combinations of mixed sedimentary styles in the second Member of the Kongdian Formation in the Cangdong Sag [20]. Additionally, the Milankovitch cycle of global evolution determines the origin of the organic matter laminae in the upper Es4 Member in the Dongying Sag. Organic-rich lamina argillaceous limestone lithofacies are the most favorable target for shale oil exploration [21].

A number of studies have shown that the lamination texture not only affects the organic matter abundance, lithology, and mineralogy of the shales [17,22,23], but also has a direct effect on the volumetric fracture propagation law and the fracturing effect of the horizontal wells directly [24–26]. Some scholars proposed that there is a crucial disparity in organic matter content between the mud laminae and the silt laminae [16]. Changes in TOC values were detected in mud laminae with mineral compositions and in silt laminae with different thicknesses [23,27]. On the whole, however, little attention has been paid to the influence of lamination texture on shale reservoir properties. Previous research on the second Member of the Kongdian Formation in the Cangdong Sag has tended to focus on the favorable lithofacies and intervals from the perspective of lithology and lithofacies of the second Member of the Kongdian Formation in the Cangdong Sag. For example, based on XRD data and sedimentary structural characteristics, seven types of shale—laminated felsic shale, massive felsic shale, lump felsic shale, laminated limy dolomite, massive limy dolomite, laminated hybrid shale, and massive hybrid shale—were identified in the second Member of the Kongdian Formation [28]. Subsequently, others proposed a four-fold model—thinly-bedded dolomitic shale, lamellar mixed shale, lamellar felsic shale, and bedded dolomitic shale—according to the dominant rock types, rhythmic structures, and logging curve characteristics [29]. To clarify this situation, it is vital to carry out a correlated study of the influence of lamination texture on reservoir quality characterization.

In this study, organic geochemical analysis, X-ray diffraction analysis, thin section identification, and field emission scanning electron microscopy identification are used to examine the lamina types and combination characteristics of the fine-grained hybrid shale

in the second Member of the Kongdian Formation in the Cangdong Sag and to study the pore structures corresponding to different lamina types. The study focuses on the influence of the lamination texture on the reservoir properties of the shale strata, and the vertical distribution characteristics of lamina combinations. The conclusions will not only provide valuable guidance for shale oil exploration and development in the study area but will also supplement the geological theory and support the technological development of lacustrine shale oil reservoir evaluation and sweet spots optimization.

## 2. Geological Settings

The Cangdong Sag is located in the Bohai Bay Basin of eastern China. It is a Cenozoic inland depression basin [27,30,31]. The Kongdian Formation in the sag is divided into three members. The second Member of the Kongdian Formation, with a thickness of 400–600 m, was deposited during the period of greatest flooding, when abundant organic-rich shale and a small amount of siltstone, medium sandstone, and argillaceous dolomite were deposited [32–34]. The sedimentary environment changed regularly, from semi-arid to warm and humid, and then to arid and hot, in a freshwater-brackish, partially reductive inland closed basin [27,35]. The sedimentary facies transformed from delta plains and delta front facies in the basin margin—a conventional sandstone area dominated by medium-fine sandstone—to semi-deep and deep lacustrine facies in the central part of the basin, a major hydrocarbon-source rock area dominated by shale, and a transitional zone of coastal-shallow lacustrine facies dominated by argillaceous siltstone and silty mudstone (Figure 1).

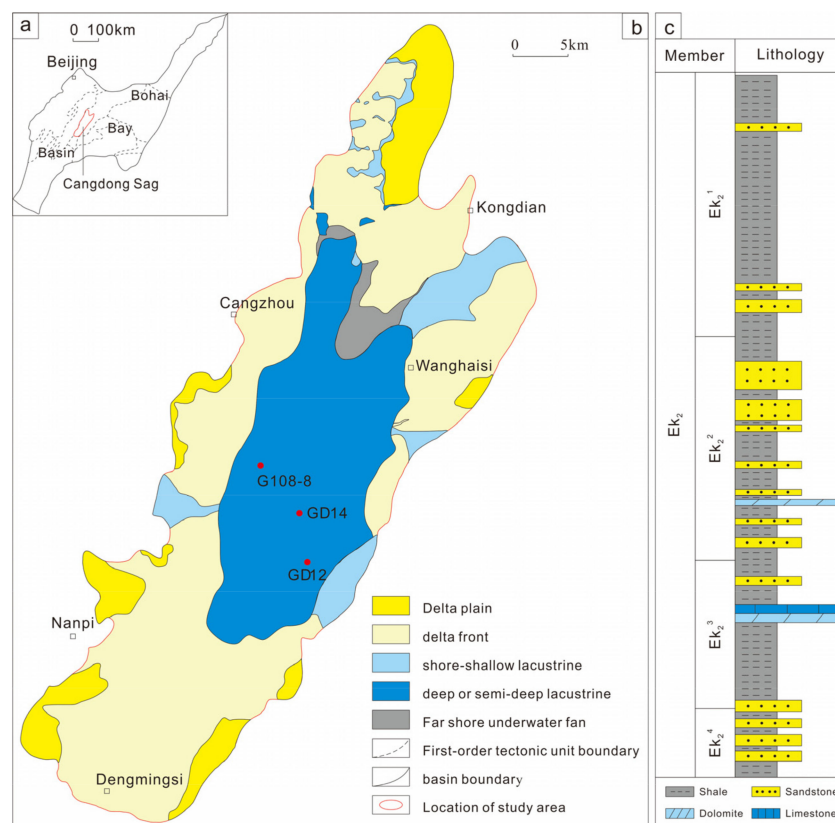


**Figure 1.** Areal distribution of sedimentary facies and stratigraphy development of the study area (modified after [27]). (a) The location of the Cangdong Sag in the Bohai Bay Basin; (b) areal distribution map of sedimentary facies of the second Member of Kongdian Formation; (c) stratigraphy development of the second Member of Kongdian Formation.

Shale strata in the second Member of the Kongdian Formation in the Cangdong Sag have a high abundance of organic matter, with total organic carbon content (TOC) of more than 1% and a maximum of 11.5%. Kerogen is mainly Types I and II<sub>1</sub> with a moderate degree of thermal maturity, Ro ranging from 0.6% to 1.2%, average S<sub>1</sub> of 2.5 mg/g, and average OSI of 105.2 mg/g. S<sub>2</sub> is greater than 3 mg/g overall, with an average 20.1 mg/g (Figure 2a,b). The strata show frequently vertical variations and complicated mineral compositions [36], with varying contents of quartz, feldspar, calcite, dolomite, analcite, pyrite, and a variety of clay minerals, which shows the pattern of ‘high carbonate content, low clay mineral content’ (Figure 2c). The carbonate is mainly dolomite with an average content of over 30%. Clay mineral content mainly varies from 10% to 30%, with an average of 21.1%. The reservoir is dense, with porosity generally less than 6% and an average of 3.72%. The average permeability is 1.66 mD, and the proportion of samples with permeability less than 0.1 mD is 43.6% (Figure 2d).

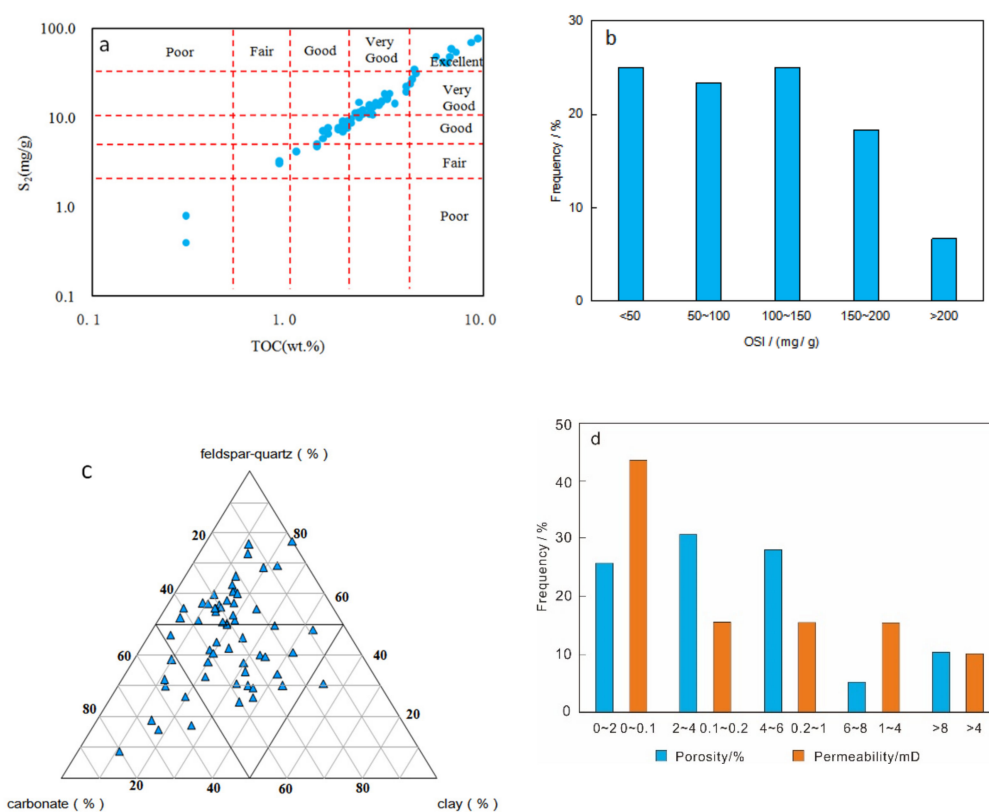


**Figure 2.** (a) Pyrolysis S<sub>2</sub> (the pyrolyzate amount released from kerogen) versus total organic carbon (TOC) plot diagram (modified after [37]); (b) frequency histogram of OSI; (c) ternary plots of mineral contents of the second Member of Kongdian Formation in Cangdong Sag. (d) Porosity and permeability.

### 3. Samples and Methods

The core samples used in the study were taken from three wells drilled in the deep lacustrine facies of the Cangdong Sag—Well Guan 108-8, Well Guandong 12, and Well Guandong 14—with a total of 60 sections. First, rock thin sections identification, TOC, rock pyrolysis, and X-ray diffraction (XRD) mineral composition were performed on the samples. Microscopic rock characterization was then carried out using a polarized light microscope to identify lamina types. At the same time, representative samples were chosen for field emission scanning electron microscopy (SEM) studies to examine the pore structures of different laminae. Finally, combining the research results, differences in mineral composition, organic geochemical characteristics, and pore structures in different

laminae were summarized, as well as their vertical distribution characteristics. The key experimental methods are as follows.

### 3.1. TOC and Rock Pyrolysis Analysis

TOC content and rock pyrolysis analysis were carried out in the Key Laboratory of Petroleum Geochemistry of China National Petroleum Corporation (Beijing, China), using a CS-i Carbon and Sulfur Analysis instrument to test the TOC of the 200-mesh powder samples under normal temperature and pressure conditions. Rock thermal pyrolysis was performed using a Rock Eval 6 instrument, also on 200-mesh powder samples.

### 3.2. Polarization Microscope, X-ray Diffraction, and Field Emission Scanning Electron Microscope Analysis

Optical microscope, X-ray diffraction mineral analysis, and field emission scanning electron microscope analysis were conducted in the National Energy Tight Oil and Gas Research and Development Center using a polarized light microscope from LEICA (DM4500P, Wetzlar, Germany). Thin sections, made by polishing or grinding the rock samples, were viewed under single-polarization and orthogonal polarization with the magnifications between 20x and 400x.

X-ray diffraction analysis of rock minerals was performed using a Rigaku Smart Lab diffractometer with a working voltage of 45 kV and working current of 150 mA. A TTR instrument was used for XRD clay mineral analysis, with a working voltage of 48 kV and working current of 100 mA.

Argon ion polishing of samples was done in a Leica REC. After being sprayed with carbon, the samples were observed in an FEI Apreo high-resolution field emission scanning electron microscope. The imaging working voltage, working current, and working distance were 5 kV, 0.4 nA, and 4.0 mm, respectively. EDS energy spectrum analysis was performed on a Bruker (Czechoslovakia) energy spectrometer with a working voltage, working current, and working distance of 10 kV, 0.8 nA, and 10.0 mm, respectively.

To further study differentiation in the pore structures of different laminae, the Apreo field emission scanning electron microscope made by FEI was used to carry out a large field of view stitching study, using SEM large area mosaic imaging technology (MAPS), with a working voltage, working current, and working distance of 5 kV, 0.4 nA, and 4.0 mm, respectively. The pixel resolution of the resulting images was 10 nm, and 300–500 images were obtained for each sample. Using the watershed method, AVIZO image processing software was used to identify pores and the equivalent circle model was applied to calculate parameters such as pore diameter and thin section porosity.

## 4. Results and Discussion

### 4.1. Laminae Types and Their Combinations

Under the optical microscope, five types of laminae were identified in the second Member of the Kongdian Formation, each displaying different optical characteristics, thicknesses, and combination propensities: clay laminae, feldspar-quartz laminae, carbonate laminae, organic matter laminae, and bioclastic laminae.

Feldspar-quartz laminae are colorless under plane-polarized light, and a small amount of dispersed organic matter can be seen. Parts of the laminae show insufficient purity for the development of plentiful interstitial clay minerals (Figure 3a,b). The thickness of a single lamina mainly varies within the range of 200–1000  $\mu\text{m}$ , with horizontal and microwave-like shapes which showed small fluctuations. The boundaries between feldspar-quartz laminae are not obvious, and they are generally interbedded with the clay laminae.

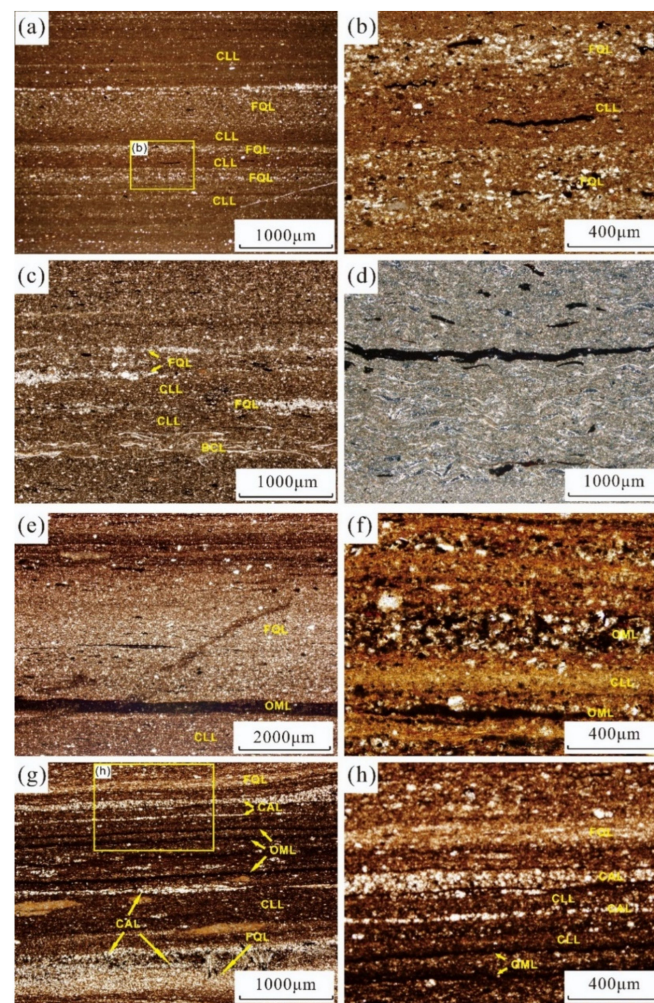


**Figure 3.** Optical microscope images of different laminae of the second Member of Kongdian Formation in the Cangdong Sag. (a,b) Combination of FQL and CLL, the CLL interbedded with the FQL, plane-polarized light; (c) combination of FQL, CLL, and BCL, the CLL interbedded with the FQL and the BCL, plane-polarized light; (d) BCL, straight or arc shape, cross-polarized light; (e,f) combination of FQL, CLL, and OML, plane-polarized-light; (g,h) combination of FQL, CAL, CLL, and OML, the CLL interbedded with the FQL, CAL, and OML, plane-polarized light. FQL: feldspar-quartz laminae; CLL: clay laminae; CAL: carbonate laminae; OML: organic matter laminae; BCL: bioclastic laminae.

The most widespread type of laminae in the second Member of the Kongdian are clay laminae. These are brown and dark under plane-polarized light, with the thicknesses ranging from tens to several thousand  $\mu\text{m}$ . They generally occur alongside feldspar-quartz laminae, showing a ‘rhythmic bedding’ texture with varying grain sizes. Various forms of organic matter can be observed in clay laminae (Figure 3a,b).

Bioclastic laminae are composed of calcite, quartz, feldspar, and clay minerals, displaying a combination of multi-layer three-dimensional distribution and single-layer-oriented arrangements. The thickness of the bioclasts with the straight or arc shapes ranges from 10 to 20  $\mu\text{m}$  while the length is about 100–500  $\mu\text{m}$  (Figure 3c,d). In general, development of bioclastic laminae alongside feldspar-quartz laminae and clay laminae is uncommon.

Organic matter laminae are dark or black under plane-polarized light. They generally have a dispersed distribution when the TOC is relatively low, but are mostly horizontally bedded, with continuous or intermittent distribution when the TOC is high (Figure 3e,f). Organic matter presents as enriched laminae, alternated with the carbonate laminae or

clay laminae, and can also occur in other laminae in the shape of short lines with clear boundaries. Organic matter laminae are rather thin and generally vary from 20  $\mu\text{m}$  to 40  $\mu\text{m}$ .

Calcite and dolomite laminae are collectively referred to as carbonate laminae. They display a high-grade white interference color under the cross-polarized light, and generally have a thickness of less than 100  $\mu\text{m}$  (Figure 3g,h). Morphologically, they display intermittent, microwave-like features, with obvious transverse undulations and great variations in thickness and are interbedded with clay laminae.

The five types of laminae can occur in four combinations: FQL-CLL combination (Figure 3a), FQL-CLL-BCL combination (Figure 3c), FQL-CLL-OML combination (Figure 3e), and FQL-CAL-CLL-OML combination (Figure 3g).

#### 4.2. Lamination Texture Characterization

##### 4.2.1. Differences in Mineral Compositions of Lamination Texture

Previous studies have revealed that the mineral compositions of different laminae vary considerably. This study therefore focuses on differences in the mineral compositions of lamina combinations. Mineral analysis of X-ray diffraction indicates that the content of carbonate minerals in different lamina combinations is fairly consistent, but that of felsic minerals and clay minerals varies considerably. In the FQL-CLL combination, the content of felsic minerals content is up to 36%—and the content of the clay mineral and carbonate minerals are 25% and 27%, respectively, whereas the pyrite is fairly low (Figure 4a). Felsic minerals, clay minerals, and carbonate minerals account for 39%, 27%, and 18% in the FQL-CLL-BCL combination, respectively (Figure 4b), indicating a high content of felsic minerals, low content of clay minerals, and prominent plagioclase in this combination type. In the FQL-CLL-OML combination, the proportions of felsic minerals, clay minerals, and carbonate minerals are 26%, 25%, and 25%, respectively, with a high analcite content (about 22%) (Figure 4c); in the FQL-CAL-CLL-OML combination, the content of minerals tends to be high clay and low analcite, with felsic minerals, clay minerals, and carbonate minerals accounting for 29%, 42%, and 24%, respectively (Figure 4d).

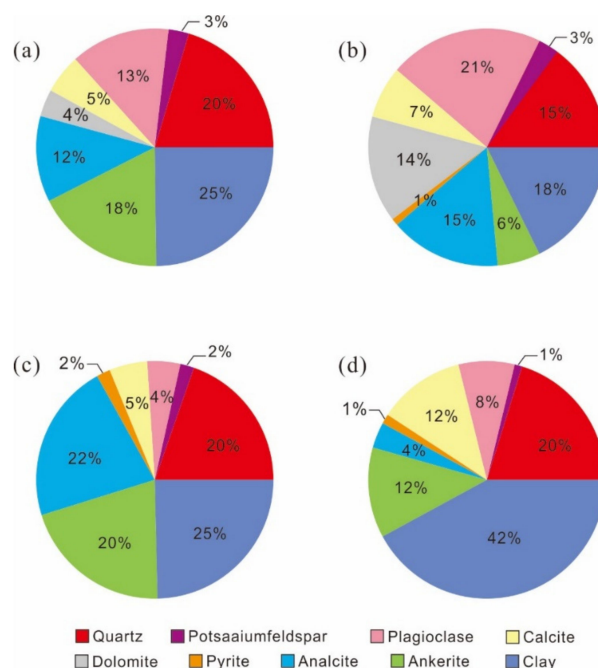


**Figure 4.** Mineralogy of the second Member of Kongdian Formation in Cangdong Sag. (a) Combination of FQL and CLL; (b) combination of FQL, CLL, and BCL; (c) combination of FQL, CLL, and OML; (d) combination of FQL, CAL, CLL, and OML. FQL: feldspar-quartz laminae; CLL: clay laminae; CAL: carbonate laminae; OML: organic matter laminae; BCL: bioclastic laminae.

#### 4.2.2. Organic Geochemical Characteristics of Lamination Texture

Once the laminae were identified, the TOC and rock pyrolysis analysis data of the samples were conducted, with the results showing good agreement between the TOC and specific laminae combinations (Figure 5). TOC of the FQL-CLL combination ranges from 2.1% to 4.4%, with an average value of 3.0%; TOC of the FQL-CLL-BCL combination ranges from 1.9% to 5.7%, with an average of 3.4%; TOC of the FQL-CLL-OML combination ranges from 2.0% to 9.3%, with an average of 5.1%; and TOC of the FQL-CAL-CLL-OML combination ranges from 3.2% to 8.6% with an average of 6.3%. Overall, variations in TOC between the combinations are consistent and can be quantitatively expressed as follows: FQL-CAL-CLL-OML > FQL-CLL-OML > FQL-CLL-BCL > FQL-CLL.

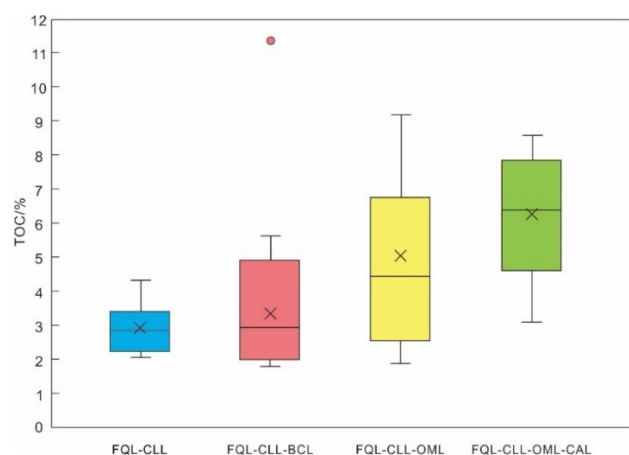


**Figure 5.** Box plots of TOC in different laminae combinations, occurrence of an outlier in the FQL-CLL-BCL combination. FQL: feldspar-quartz laminae; CLL: clay laminae; CAL: carbonate laminae; OML: organic matter laminae; BCL: bioclastic laminae.

#### 4.2.3. Pore Structures of Lamination Texture

Previous studies have shown that the differences in pore texture have an important impact on shale oil storage capacity and microscopic seepage capacity [38–42]. In the present study, apparent differences in pore types and pore structures between different laminae can be distinguished under field emission scanning electron microscopy. A comparison reveals the following.

##### Feldspar-Quartz Laminae

Feldspar-quartz laminae are principally composed of feldspar, quartz, pyrite, and a small amount of scattered organic matter, with relatively coarse grain size and strong diagenetic cementation (Figure 6a). Interstitial clay minerals are formed between feldspar and quartz particles. The pores are predominantly intercrystalline pores of clay minerals, mostly chlorite (Figure 6a). Internal pores and dissolved pores of feldspar and other minerals are less developed. Chlorite intercrystalline pores are widely dispersed in strips, with great variations in pore diameters. Feldspar-quartz laminae, which have no developed microfractures or organic pores, are mostly nano-pores that rarely exceed 10  $\mu\text{m}$  in diameter (Figure 6c).

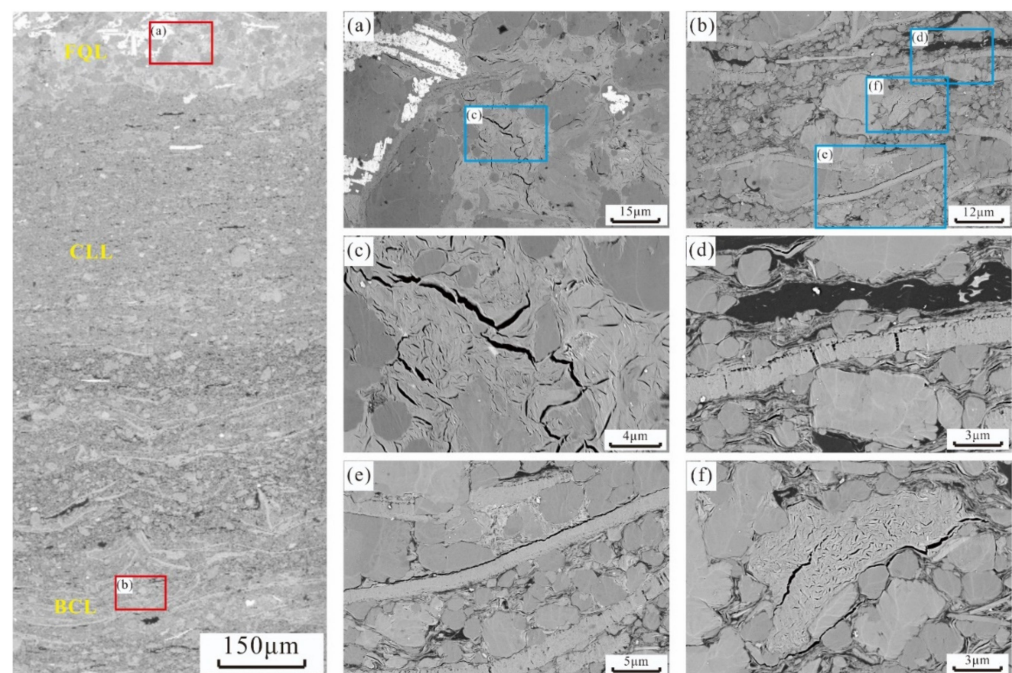


**Figure 6.** SEM images of FQL and BCL from Well G108-8 at 2936.73 m. (a) Magnification of FQL; (b) magnification of BCL; (c) intercrystalline pores of clay minerals in FQL; (d) intercrystalline pores of bioclastic in BCL; (e) edge gap of bioclastic in BCL; (f) intercrystalline pores of clay minerals in BCL. FQL: feldspar-quartz laminae; CLL: clay laminae; BCL: bioclastic laminae.

#### Bioclastic Laminae

Quartz, feldspar, calcite, and clay minerals, combined with organic matter, are easily identified in bioclastic laminae (Figure 6b). The bioclasts form bands, and the interstitial clay minerals fill between the feldspar and quartz particles. Intercrystalline pores of clay minerals (mostly chlorite), internal pores of bioclastic grains, and the microcracks at the edges of the bioclasts are well developed. There are comparatively few dissolution pores and organic matter pores (Figure 6d–f). Chlorite intercrystalline pores, with great variations in pore diameters, are densely distributed and generally elongated, with a small number of pores extending over 5 μm (Figure 6f). Internal pores in bioclastic particles are round and elliptical, and densely arranged (Figure 6d). Microcracks, (also called shell edge cracks), flat or slightly curved in shape, occur at the contact interface between bioclastic and other minerals, with length-to-width ratios greater than ten, and the extension lengths of more than 30 μm (Figure 6e).

#### Carbonate Laminae

Carbonate laminae are mostly dolomite (or calcite) with small amounts of scattered pyrite, and are relatively coarse grained. Clay minerals and organic matter occur between the dolomite particles (Figure 7a). The pores are mostly intercrystalline nano-pores of clay minerals, supplemented by organic pores. Intragranular pores or dissolution pores such as feldspar are less developed, with very few microcracks (Figure 7b). Intercrystalline pores in the clay minerals develop in chlorite aggregates and are elongated, triangular, or irregular in shape (Figure 7c). Organic matter pores are spherical and ellipsoidal, and dispersed in interstitial organic matter (Figure 7c).

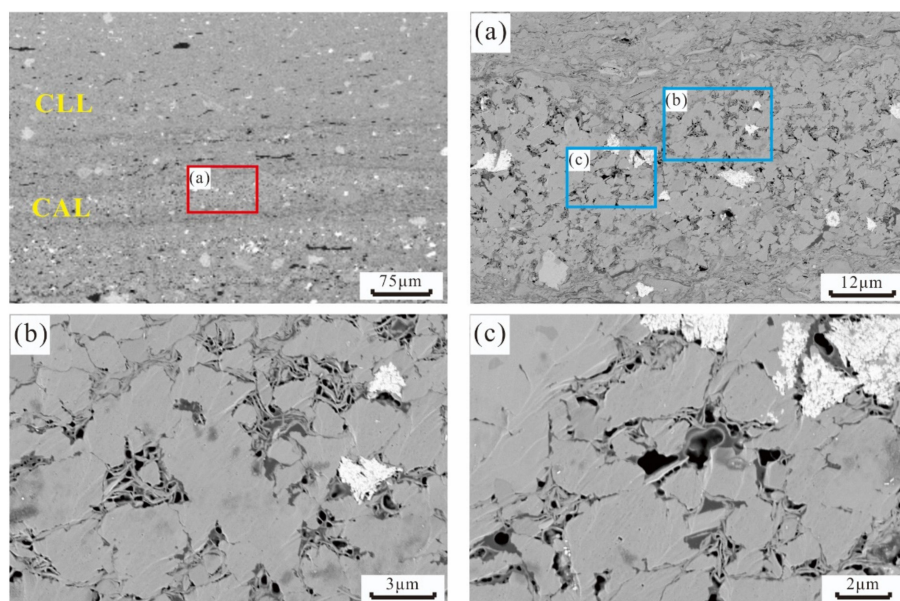


**Figure 7.** SEM images of CAL from Well G108-8 at 3209.43 m. (a) Magnification of CAL; (b) intercrystalline pores of clay minerals in CAL; (c) organic pores in CAL. CLL: clay laminae; CAL: carbonate laminae.

### Clay Laminae

Clay laminae generally consist of clay minerals, feldspar, quartz, and large amounts of organic matter, with strong diagenetic cementation (Figure 8a,c). Organic matter develops in the form of lumps, bands, and interstitials with few intragranular pores (feldspar, etc.) and corrosion pores. Organic pores have dispersed distribution and occur in elliptical, triangular, or irregular shapes. They are generally of nano-scale, with diameters of less than 1 µm (Figure 8b). The degree of microcracking is low.

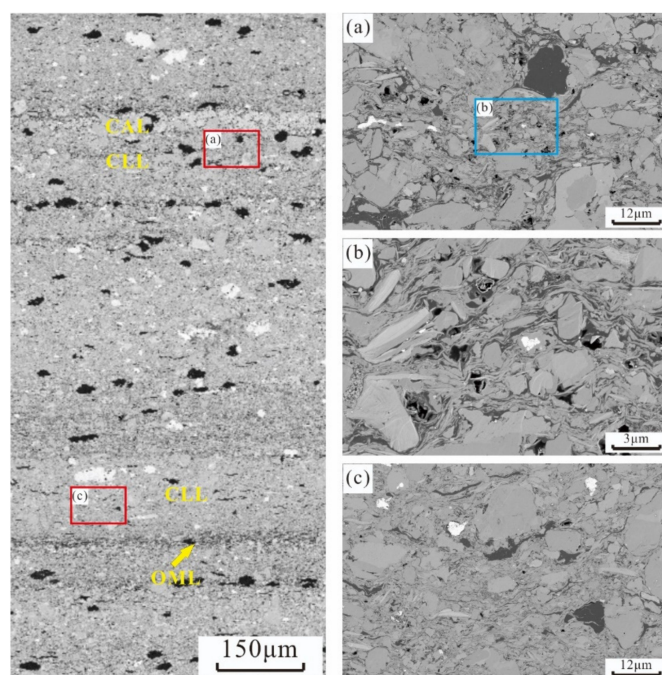


**Figure 8.** SEM images of CLL from Well G108-8 at 3212.64 m. (a,c) Magnification of CLL; (b) organic pores in CLL. CLL: clay laminae; CAL: carbonate laminae; OML: organic matter laminae.

### Organic Matter Laminae

Organic matter laminae are gray-black in appearance under a field emission scanning electron microscope, with relatively coarse grains. Quartz and feldspar develop between organic matter stripes, along with a low content of clay minerals, with strong diagenetic cementation (Figure 9). Pores in the organic matter laminae are predominantly intercrystalline pores of clay minerals and shrinkage pores of organic matters. There are relatively few intragranular pores of feldspar and other minerals, or dissolution pores (Figure 9a). Shrinkage pores of organic matter develop at the contact interface between organic matter and feldspar minerals, around the boundaries between minerals. Their length-to-width ratio is greater than ten, with farther extension (Figure 9b). Intercrystalline pores of clay minerals occur in long strips, and are generally less than 3  $\mu\text{m}$  in length (Figure 9c). Overall, pores in organic matter laminae are nano-scale.

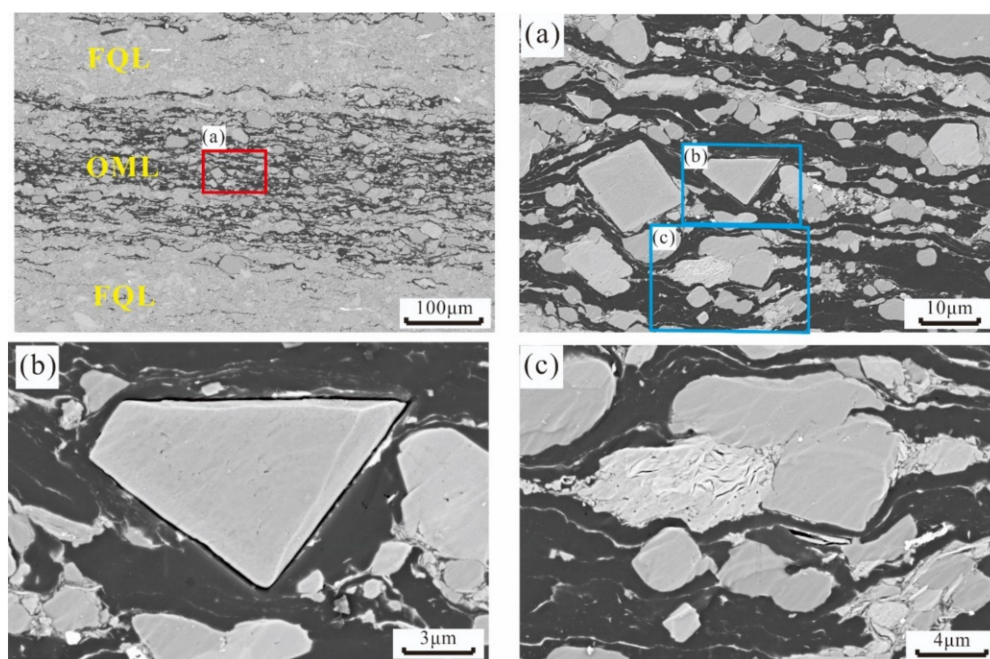


**Figure 9.** SEM images of OML from Well G108-8 at 2956 m. (a) Magnification of OML; (b) organic matter pores; (c) intercrystalline pores of clay minerals in OML. FQL: feldspar-quartz laminae; OML: organic matter laminae.

The five types of laminae were scanned using SEM large area mosaic imaging technology (MAPS) to calculate the equivalent pore diameters and thin section porosity in field view (Figure 10). Statistically, the equivalent diameters of pores show that the second Member of the Kongdian Formation in the Cangdong Sag is dominated by mesopores, with an equivalent diameter mainly less than 50 nm. The equivalent diameters of pores in feldspar-quartz laminae and clay laminae are relatively large, while 87% of the equivalent diameters of pores in carbonate laminae are less than 10 nm (Figure 10).

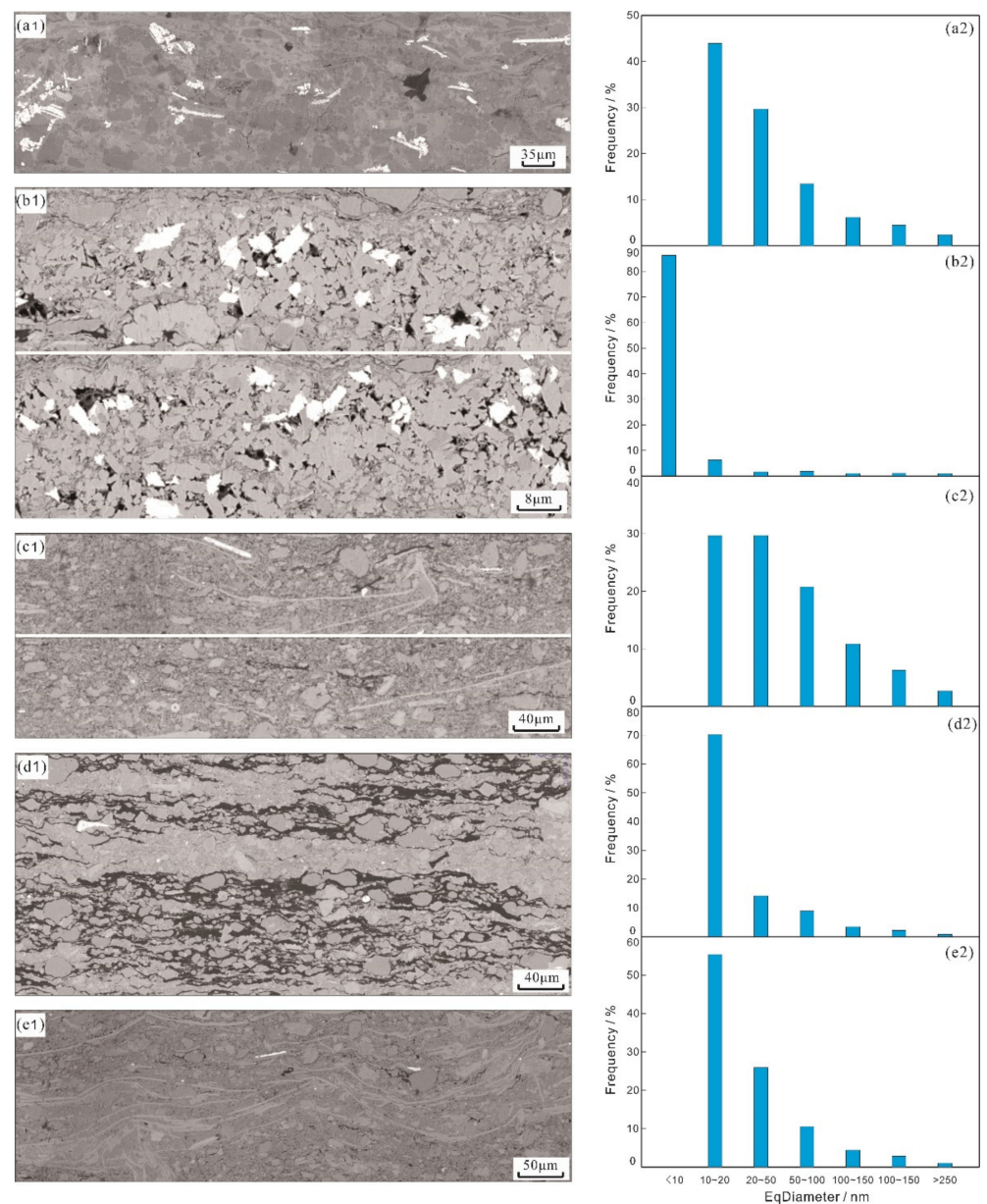


**Figure 10.** MAPS images and equivalent diameter of pores in different laminae. (a1,a2) MAPS images and equivalent diameter of pores in feldspar-quartz laminae; (b1,b2) MAPS images and equivalent diameter of pores in carbonate laminae; (c1,c2) MAPS images and equivalent diameter of pores in clay laminae; (d1,d2) MAPS images and equivalent diameter of pores in organic matter laminae; (e1,e2) MAPS images and equivalent diameter of pores in bioclastic laminae.

Thin section porosity data show an obvious correlation to laminae, with comparison of thin section porosity as follows: carbonate laminae > feldspar-quartz laminae > organic matter laminae > bioclastic laminae > clay laminae. The mean values obtained are 0.90%, 0.16%, 0.15%, 0.10%, and 0.01%, respectively (Figure 11).

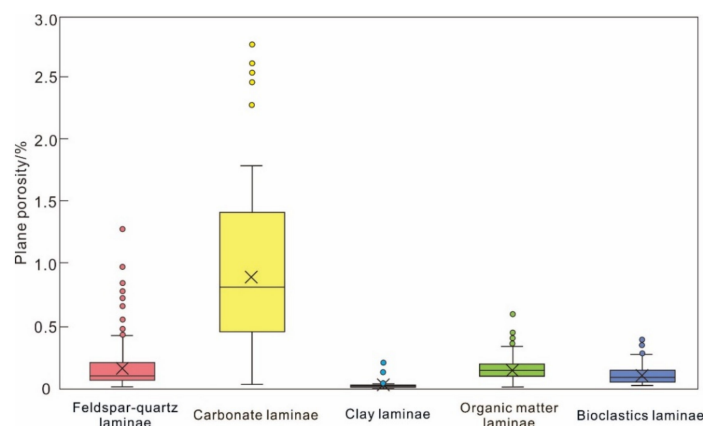


Figure 11. Box plot of thin section porosity in different laminae.

Thin section porosity in carbonate laminae is by far the highest, but the equivalent pore diameter is smaller than in feldspar-quartz laminae and clay laminae. This may be explained by differences in the distributions of pores. Pores in carbonate laminae are small in size but relatively densely distributed, and the quantity of pores is much higher than in other laminae. Compared with feldspar-quartz laminae and clay mineral laminae with ‘large and few’ pores, the ‘small and many’ pores of the carbonate laminae contribute more to thin section porosity.

4.3. Vertical Distribution Characteristics of Laminae

In the present study, the mineral compositions and the distribution characteristics of the laminae in the second Member of the Kongdian Formation in the Cangdong Sag were analyzed to determine the vertical variations in the mineral compositions and distribution of the laminae (Figure 12). Mineral composition analysis shows an apparent decrease in clay minerals and increase in felsic minerals, as well as slight fluctuations in carbonate minerals between the lower part of the second Member of the Kongdian Formation and the upper part.

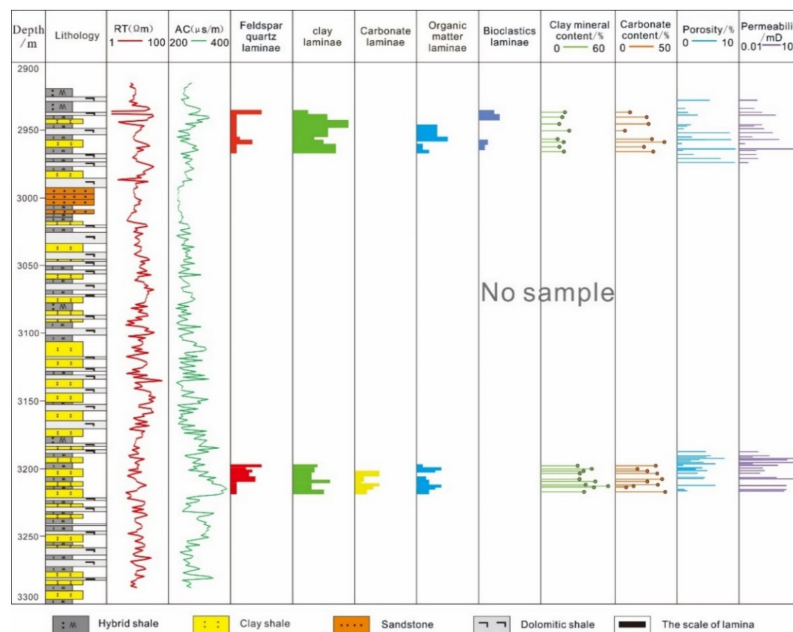


Figure 12. Laminae distribution of Well G108-8 in the second Member of the Kongdian Formation in Cangdong Sag.

Three types of laminae combination of FQL-CLL, FQL-CLL-BCL, and FQL-CLL-OML occur in the upper second Member of the Kongdian Formation, while lamina combinations of the lower second Member of the Kongdian Formation are predominantly FQL-CLL, FQL-CLL-OML, and FQL-CAL-CLL-OML. On the whole, feldspar-quartz laminae and clay laminae are developed throughout the second Member of the Kongdian Formation. Bioclastic laminae are typically found in the upper part, and carbonate laminae occur mainly in the lower part.

## 5. Conclusions

In this study, the laminae types and combinations found in the second Member of the Kongdian Formation in the Cangdong Sag, Bohai Bay Basin are analyzed and their effects on reservoir properties determined by an integrated approach, including petrology, mineralogy, organic geochemistry, and reservoir evaluation techniques. The principal findings are as follows:

- (1) The second Member of the Kongdian Formation in the Cangdong Sag has five types of laminae: feldspar-quartz laminae (FQL), clay laminae (CLL), carbonate laminae (CAL), organic matter laminae (OML), and bioclastic laminae (BCL). The laminae occur in four combinations: FQL-CLL, FQL-CLL-BCL, FQL-CLL-OML, and FQL+CAL+CLL+OML.
- (2) The differences in mineral composition between the laminae combinations are generally variations in the contents of felsic and clay minerals, while carbonate mineral content varies only slightly. TOC has an obvious correlation with lamination texture that provides a crucial basis for hydrocarbon source potential analysis, with the consistent trend being: FQL-CAL-CLL-OML > FQL-CLL-OML > FQL-CLL-BCL > FQL-CLL.
- (3) There are marked disparities in pore types and distribution between different laminae. The pores in FQL, CAL, BCL, and OML are mostly intercrystalline pores of clay minerals. Organic pores are well developed in CAL and CLL, and intragranular pores of bioclastic minerals in BCL. The pores are predominantly mesopores. The equivalent diameter of pores in feldspar-quartz laminae and clay laminae is ascendant, precisely opposite to the equivalent diameter of pores in carbonate laminae. The comparative thin section porosities of laminae can be characterized as: carbonate laminae > feldspar-quartz laminae > organic matter laminae > bioclastic laminae > clay laminae. Carbonate laminae with 'small but many' pore characteristics contribute the highest proportion to thin section porosity.
- (4) Differentiation between vertical distributions of laminae is accomplished in a single well. FQL and CLL are widely distributed across all the samples, while BCL is concentrated in the upper part of the second Member of the Kongdian Formation, and CAL in the lower part.

**Author Contributions:** Conceptualization, S.H. and R.Z.; methodology, S.W.; formal analysis, M.L. and S.W.; investigation, M.L.; resources, S.W., R.Z. and S.M.; writing—original draft preparation, M.L. and S.W.; writing—review and editing, S.W.; visualization, J.Y.; supervision, S.W.; project administration, R.Z. and S.W.; funding acquisition, R.Z. All authors have read and agreed to the published version of the manuscript.

**Funding:** This work is supported by a Major Science and Technology Project of China National Petroleum Corporation [Grant No. 2019E-2601,2021DQ0405].

**Data Availability Statement:** Data will be made available upon request.

**Acknowledgments:** The authors would like to thank Lihua Ding, Fulin Zhai, Huadong Li, Xiaohua Jiang, Ganlin Hua, and Xiaohong Li from CNPC, Beijing, China, for their help during the sample analysis. We appreciate the valuable comments from the editors and anonymous reviewers.

**Conflicts of Interest:** The authors declare that they have no known competing financial interests or personal relationships that could have appeared to influence the work reported in this paper.

## References

1. Stow, D.A.V.; Bowen, A.J. Origin of lamination in deep sea, fine-grained sediments. *Nature* **1978**, *274*, 324–328. [[CrossRef](#)]
2. Schieber, J. Reverse engineering mother nature-Shale sedimentology from an experimental perspective. *Sediment. Geol.* **2011**, *238*, 1–22. [[CrossRef](#)]
3. Zhao, W.Z.; Hu, S.Y.; Hou, L.H.; Yang, T.; Li, X.; Guo, B.C.; Yang, Z. Types and resource potential of lacustrine shale oil in China and its boundary with tight oil. *Pet. Explor. Dev.* **2020**, *47*, 1–10. [[CrossRef](#)]
4. Hu, S.Y.; Zhao, W.Z.; Hou, L.H.; Yang, Z.; Zhu, R.K.; Wu, S.T.; Bai, B.; Jin, X. Development potential and technical strategy of lacustrine shale oil in China. *Pet. Explor. Dev.* **2020**, *47*, 819–828. [[CrossRef](#)]
5. Jin, Z.J.; Bai, Z.R.; Gao, B.; Li, M.W. Has China ushered in the shale oil and gas revolution. *Oil Gas Geol.* **2019**, *40*, 451–458.
6. Zou, C.N.; Pan, S.Q.; Jing, Z.H.; Gao, J.L.; Yang, Z.; Wu, S.T.; Zhao, Q. Shale oil and gas revolution and its impact. *Acta Pet. Sin.* **2020**, *41*, 1–12.
7. Li, G.X.; Zhu, R.K. Progress, challenges and key issues of unconventional oil and gas development of CNPC. *China Pet. Explor.* **2020**, *25*, 1–13.
8. Hou, L.H.; Ma, W.J.; Luo, X.; Liu, J.Z.; Lin, S.H.; Zhao, Z.Y. Hydrocarbon generation-retention-expulsion mechanism and shale oil producibility of the Permian Lucaogou shale in the Junggar Basin as simulated by semi-open pyrolysis experiments, *Mar. Pet. Geol.* **2021**, *125*, 1–12. [[CrossRef](#)]
9. Liu, G.H.; Huang, Z.L.; Jiang, Z.X.; Chen, J.F.; Chen, C.C.; Gao, X.Y. The characteristic and reservoir significance of lamina in shale from Yanchang Formation of Ordos Basin. *Nat. Gas Geosci.* **2015**, *26*, 408–417.
10. Campbell, C.V. Lamina, laminaset, bed and bedset. *Sedimentology* **1967**, *8*, 7–26. [[CrossRef](#)]
11. MAacquaker, J.H.S.; Keller, M.A.; Davies, S.J. Algal blooms and “marine snow”: Mechanisms that enhance preservation of organic carbon in ancient fine-grained sediments. *J. Sediment. Res.* **2010**, *80*, 934–942. [[CrossRef](#)]
12. Lazar, O.R.; Bohacs, K.M.; Macquaker, J.H.S.; Schieber, J.; Demko, T.M. Capturing key attributes of fine-grained sedimentary rocks in outcrops, cores, and thin sections: Nomenclature and description guidelines. *J. Sediment. Res.* **2015**, *85*, 230–246. [[CrossRef](#)]
13. Ingram, R.L. Terminology for the thickness of stratification and parting units in sedimentary rocks. *GSA Bull.* **1954**, *65*, 937–938. [[CrossRef](#)]
14. Dong, C.M.; Ma, C.F.; Lin, C.Y.; Sun, X.; Yuan, M.Y. A method of classification of shale set. *J. China Univ. Pet. (Ed. Nat. Sci.)* **2015**, *39*, 1–7.
15. Liu, H.M.; Wang, Y.; Yang, Y.H.; Zhang, S. Sedimentary environment and Lithofacies of fine-grained hybrid in Dongying Sag: A case of fine-grained sedimentary system of the Es4. *Earth Sci.* **2020**, *45*, 3543–3555.
16. Xi, K.L.; Li, K.; Cao, Y.C.; Lin, M.R.; Niu, X.B.; Zhu, R.K.; Wei, X.Z.; You, Y.; Liang, X.W.; Feng, S.B. Laminae combination and shale oil enrichment patterns of Chang 73 sub-member organic-rich shales in the Triassic Yanchang Formation, Ordos Basin, NW China. *Pet. Explor. Dev.* **2020**, *47*, 1244–1255. [[CrossRef](#)]
17. Shi, Z.S.; Qiu, Z.; Dong, D.Z.; Lu, B.; Liang, P.P.; Zhang, M.Q. Laminae characteristics of gas-bearing shale fine-grained sediment of the Silurian Longmaxi Formation of Well Wuxi 2 in Sichuan Basin, SW China. *Pet. Explor. Dev.* **2018**, *45*, 339–348. [[CrossRef](#)]
18. Yawar, Z.; Schieber, J. On the origin of silt laminae in laminated shales. *Sediment. Geol.* **2017**, *360*, 22–34. [[CrossRef](#)]
19. Shi, Z.S.; Dong, D.Z.; Wang, H.Y.; Sun, S.S.; Wu, J. Reservoir characteristics and genetic mechanisms of gas-bearing shales with different laminae and laminae combinations: A case study of Member 1 of the Lower Silurian Longmaxi shale in Sichuan Basin, SW China. *Pet. Explor. Dev.* **2020**, *47*, 829–840. [[CrossRef](#)]
20. Yan, J.H.; Deng, Y.; Pu, X.G.; Zhou, L.H.; Chen, S.Y.; Jiao, Y.X. Characteristics and controlling factors of fine-grained mixed sedimentary rocks from the 2nd Member of Kongdian Formation in the Cangdong Sag, Bohai Bay Basin. *Oil Gas Geol.* **2017**, *38*, 98–109.
21. Sun, S.Y.; Liu, H.M.; Cao, Y.C.; Zhang, S.; Yang, Y.; Yang, W.Q. Milankovitch cycle of lacustrine deepwater fine-grained sedimentary rocks and its significance to shale oil: A case study of the upper Es4 member of well NY1 in Dongying sag. *J. China Univ. Min. Technol.* **2017**, *46*, 846–858.
22. Zhao, J.H.; Jin, Z.J.; Jin, Z.K.; Wen, X.; Geng, Y.K.; Yan, C.N.; Nie, H.K. Lithofacies types and sedimentary environment of shale in Wufeng-Longmaxi Formation, Sichuan Basin. *Acta Pet. Sin.* **2016**, *37*, 572–586.
23. Wang, C.; Zhang, B.Q.; Hu, Q.H.; Shu, Z.G.; Sun, M.D.; Bao, H.Y. Laminae characteristics and influence on shale gas reservoir quality of Lower Silurian Longmaxi Formation in the Jiaoshiba area of the Sichuan Basin, China. *Mar. Pet. Geol.* **2019**, *109*, 839–851. [[CrossRef](#)]
24. Heng, S.; Yang, C.H.; Guo, Y.T.; Wang, C.Y.; Wang, L. Influence of bedding planes on hydraulic fracture propagation in shale formations. *Chin. J. Rock Mech. Eng.* **2015**, *34*, 228–237.
25. Xu, D.; Hu, R.L.; Gao, W.; Xia, J.G. Effects of laminated structure on hydraulic fracture propagation in shale. *Pet. Explor. Dev.* **2015**, *42*, 523–528. [[CrossRef](#)]
26. Jiang, T.X.; Bian, X.B.; Wang, H.T.; Li, S.M.; Jia, C.G.; Liu, H.L.; Sun, H.C. Volume fracturing of deep shale gas horizontal wells. *Nat. Gas Ind.* **2017**, *37*, 90–96. [[CrossRef](#)]
27. Zhao, X.Z.; Pu, X.G.; Han, W.Z.; Zhou, L.H.; Shi, Z.N.; Chen, S.Y.; Xiao, D.Q. A new method for Lithology identification of fine grained deposits and reservoir sweet spot analysis: A case study of Kong 2 Member in Cangdong sag, Bohai Bay Basin, China. *Pet. Explor. Dev.* **2017**, *44*, 492–502. [[CrossRef](#)]

28. Pu, X.G.; Jin, F.M.; Han, W.Z.; Shi, Z.N.; Cai, A.B.; Wang, A.G.; Guan, Q.S.; Jiang, W.Y.; Zhang, W. Sweet spots geological characteristics and key exploration technologies of lacustrine shale oil: A case study of Member 2 of Kongdian Formation in Cangdong sag. *Acta Pet. Sin.* **2019**, *40*, 997–1012.
29. Han, W.Z.; Zhao, X.Z.; Jin, F.M.; Pu, X.G.; Chen, S.Y.; Mu, L.G.; Zhang, W.; Shi, Z.N.; Wang, H. Sweet spots evaluation and exploration of lacustrine shale oil of the 2nd member of Paleogene Kongdian Formation in Cangdong sag, Dagang Oilfield, China. *Pet. Explor. Dev.* **2021**, *48*, 1–10. [[CrossRef](#)]
30. Ren, J.Y.; Zhang, Q.L. Analysis of development mechanism for center anticline high in Dongying Depression. *Geotecton. Metallog.* **2004**, *28*, 254–262.
31. Li, S.Z.; Suo, Y.H.; Zhou, L.H.; Dai, L.M.; Zhou, J.T.; Zhao, F.M.; Lu, Y.; Pu, X.G.; Lou, D.; Wu, Q.; et al. Pull-apart basins within the North China craton: Structural pattern and evolution of Huanghua Depression in Bohai Bay Basin. *J. Jilin Univ. (Earth Sci. Ed.)* **2011**, *41*, 1362–1379.
32. Chen, C.W.; Xue, L.F.; Xu, X.K.; Yan, Q.H. Re-establishment of basin framework on member 2 of Kongdian Formation in Kongnan area Huanghua depression. *Acta Sedimentol. Sin.* **2007**, *25*, 511–517.
33. Dong, Q.Y.; Liu, X.P.; Li, H.X.; Liu, Z.C.; Liu, Q.X.; Dong, Q.; Zhang, Y.; Sun, X.J. Formation conditions of shale oil reservoir in the second member of Kongdian Formation in southern Kongdian area, Huanghua depression. *Nat. Gas Geosci.* **2013**, *24*, 188–198.
34. Pu, X.G.; Han, W.Z.; Zhou, L.H.; Chen, S.Y.; Zhang, W.; Shi, Z.N.; Yang, F.; Liu, S. Lithologic characteristics and geological implication of fine-grained sedimentation in second Member of the Kongdian Formation high stand system tract of Cangdong Sag, Huanghua depression. *China Pet. Explor.* **2015**, *20*, 30–40.
35. Zhao, X.Z.; Zhou, L.H.; Pu, X.G.; Jin, F.M.; Shi, Z.N.; Xiao, D.Q.; Han, W.Z.; Jiang, W.Y.; Zhang, W.; Wang, H. Favorable formation conditions and enrichment characteristics of lacustrine facies shale oil in faulted lake basin: A case study of Member 2 of Kongdian Formation in Cangdong sag, Bohai Bay Basin. *Acta Pet. Sin.* **2019**, *40*, 1013–1029.
36. Zhou, L.H.; Pu, X.G.; Chen, C.W.; Yang, F.; Xia, J.; Guan, Q.S.; Huang, C.Y. Concept, characteristics and prospecting significance of Fine-Grained sedimentary oil gas in terrestrial lake basin: A case from the second member of Paleogene Kongdian Formation of Cangdong sag, Bohai Bay Basin. *Earth Sci.* **2018**, *43*, 3625–3639.
37. Peters, K.E.; Cassa, M.R. Applied source rock geochemistry: Chapter 5: Part II. Essential elements. In *The Petroleum System—From Source to Trap: AAPG Memoir*; Magoon, L.B., Dow, W.G., Eds.; American Association of Petroleum Geologists: Tulsa, OK, USA, 1994; Volume 60, pp. 93–120. [[CrossRef](#)]
38. Zou, C.N.; Tao, S.Z.; Yuan, X.J.; Hou, L.H.; Zhu, R.K.; Gao, X.H.; Yang, C. *Characteristics of Unconventional Oil and Gas Nanopore Reservoirs and Mechanism of Continuous Oil and Gas Accumulation*; Chinese society for Mineralogy Petrology and Geochemistry: Guiyang, China, 2011.
39. Wu, S.T.; Zou, C.N.; Zhu, R.K.; Yuan, X.J.; Yao, J.L.; Yang, Z.; Sun, L.; Bai, B. Reservoir quality characterization of upper Triassic Chang 7 shale in Ordos Basin. *Earth Sci. (J. China Univ. Geosci.)* **2015**, *40*, 1810–1823.
40. Wu, S.T.; Zhu, R.K.; Cui, J.G.; Cui, J.W.; Bai, B.; Zhang, X.X.; Jin, X.; Zhu, D.S.; You, J.C.; Li, X.H. Characteristics of lacustrine shale porosity evolution, Triassic Chang 7 member, Ordos basin, NW China. *Pet. Explor. Dev.* **2015**, *42*, 185–195. [[CrossRef](#)]
41. Zhu, R.K.; Jin, X.; Wang, X.Q.; Liu, X.D.; Li, J.M.; Sun, L.; Wu, S.T.; Su, L.; Jiao, H.; Cui, J.W. Multi-scale digital rock evaluation on complex reservoir. *Earth Sci.* **2018**, *43*, 1773–1782.
42. Wu, S.T.; Lin, S.Y.; Chao, D.J.; Zhai, X.F.; Wang, X.R.; Huang, X.; Xu, J.L. Fluid mobility evaluation based on pore structure investigation in tight sandstones: Case study of Upper Triassic Chang 6 tight sandstones in Huaqing Area, Ordos Basin. *Nat. Gas Geosci.* **2019**, *30*, 1222–1232.